

Flexible Power Point Tracking Aided Power Ramp Rate Control for Photovoltaic Systems With Small Energy Storage Capacity

Hein Wai Yan¹, *Graduate Student Member, IEEE*, Gaowen Liang¹, *Graduate Student Member, IEEE*, Neha Beniwal¹, *Member, IEEE*, Ezequiel Rodriguez¹, *Member, IEEE*, Glen G. Farivar¹, *Senior Member, IEEE*, and Josep Pou¹, *Fellow, IEEE*

Abstract—Solar photovoltaic (PV) power generation inherently fluctuates due to erratic weather conditions. Although an energy storage system (ESS) can effectively mitigate these fluctuations, conventional methods require a large ESS capacity to control both increasing and decreasing rates of PV power change. This article explores an opportunity to reduce the required ESS capacity in PV power smoothing applications by delegating the power smoothing during positive irradiance transients to a flexible power point tracking algorithm. Therefore, the ESS only needs to regulate the power ramp rate during negative irradiance transients and it no longer requires the reserved capacity for positive transients. After discharging the ESS, the proposed control fully restores it without violating the allowed ramp rate. The efficacy of the proposed power ramp rate control under rapid irradiance transients is demonstrated experimentally using a laboratory-scale setup. In addition, based on simulated case studies using a specific real-field one-day irradiance profile, the proposed control allows around 64% reduction in the required ESS capacity compared to the conventional ESS-based control.

Index Terms—Energy storage system (ESS), flexible power point tracking (FPPT), photovoltaic (PV) system, PV power ramp rate control (PRRC).

NOMENCLATURE

Acronyms

BESS	Battery energy storage system.
ESS	Energy storage system.

Manuscript received 17 May 2023; revised 15 August 2023 and 10 October 2023; accepted 12 November 2023. Date of publication 16 November 2023; date of current version 22 December 2023. This work was supported by the Republic of Singapore's National Research Foundation (NRF) through the "Distributed Energy Resource Management System for Energy Grid 2.0" project at the Energy Research Institute, Nanyang Technological University, Singapore. Recommended for publication by Associate Editor D. Vinnikov. (*Corresponding author: Hein Wai Yan.*)

Hein Wai Yan and Josep Pou are with the School of Electrical and Electronic Engineering, Nanyang Technological University, Singapore 639798 (e-mail: heinwaiy001@e.ntu.edu.sg; josep.pou@ieee.org).

Gaowen Liang and Ezequiel Rodriguez are with the Energy Research Institute, Nanyang Technological University, Singapore 639798 (e-mail: gaowen001@e.ntu.edu.sg; ezequiel001@e.ntu.edu.sg).

Neha Beniwal is with GE Global Research, Niskayuna, NY 12309 USA (e-mail: neha.beniwal@ge.com).

Glen G. Farivar is with the University of Melbourne, Parkville, VIC 3052, Australia (e-mail: gfarivar@unimelb.edu.au).

Color versions of one or more figures in this article are available at <https://doi.org/10.1109/TPEL.2023.3333534>.

Digital Object Identifier 10.1109/TPEL.2023.3333534

FPPT	Flexible power point tracking.
MAF	Moving average filter.
MP	Maximum power.
MPP	Maximum power point.
MPPT	Maximum power point tracking.
PRRC	Power ramp rate control.
PV	Photovoltaic.
RPPT	Reserve power point tracking.
SC	Supercapacitor.
SoC	State of charge.

Parameters

p_{es}	ESS power.
$p_{\text{es-ref}}$	ESS power reference.
p_{pv}	PV power.
$p_{\text{pv-max}}$	PV maximum power.
$p_{\text{pv-ref}}$	PV power reference.
P_{rated}	Rated power of the PV system.
p_{total}	Total injected power into the grid.
v_{dc}	Dc-link voltage.
v_{es}	ESS voltage.
$V_{\text{es-rated}}$	ESS rated voltage.
v_{pv}	PV voltage.
$v_{\text{pv-ref}}$	PV voltage reference.
V_{step}	PV voltage-step.
i_{es}	ESS current.
$i_{\text{es-ref}}$	ESS current reference.
i_{pv}	PV current.
i_{total}	Total injected current into the grid.
SoC	State-of-charge of the ESS.
SoC_r	State-of-charge reference.
DoD_m	Midpoint of depth-of-discharge.
Mode_{pv}	PV operation mode.
Mode_{es}	ESS operation mode.
$R(t)$	PV power ramp rate.
R_{limit}	Ramp rate limit.
P_{limit}	Ramp power limit.
T	Sampling period.
E_{es}	ESS rated capacity.
dp/dv	Slope of the P-V curve.
Thr	Threshold for dp/dv .

f_{sw}	Converter switching frequency.
f_{pv}	PV control sampling frequency.
C_{pv}	PV-side capacitor.
L_{pv}	PV dc–dc converter inductance.
L_{es}	ESS dc–dc converter inductance.

I. INTRODUCTION

ENVIROMENTAL concerns and technology advancements are driving exponential growth in renewable PV clean energy generation. Approximately 942 GW of solar PV capacity has been installed globally based on the latest renewable status report in [1]. However, due to the intermittent nature of solar irradiance caused by cloud cover, PV power generation fluctuates. These sudden fluctuations in PV power have the potential to cause significant grid voltage deviations and pose challenges in maintaining the power grid stability, especially in weak distribution grids with high PV penetration [2]. Therefore, it is necessary to regulate abrupt changes in PV power generation within the limits allowed by the grid codes [3], [4], [5].

Improving the PV control with FPPT algorithms is a cost-effective way to address this issue [6], [7], [8]. The PV system extracts the MP using MPPT as long as the PV power fluctuations are within the acceptable limits. Otherwise, the PV system operates with FPPT to regulate the PV power increment with a controlled ramp rate. However, this approach is only effective in mitigating the positive slope fluctuations in PV power since the PV control saturates at the MP under irradiance reduction, leading to uncontrolled PV power [7], [8]. To address this issue, the PV power generation is curtailed using FPPT in [9] to reserve certain capacity as a virtually stored energy for negative slope irradiance transients. An algorithm that performs FPPT while simultaneously providing the reserve power information, i.e., RPPT, has also been introduced in [10]. Nevertheless, the PV control with RPPT can regulate the PV power reduction only if the available reserve power is sufficient enough to compensate for the PV power change. Hence, this method is impractical for large irradiance transients with negative slopes. To address this issue, a forecast-based strategy has been developed in [11] that preemptively decreases the PV power with a controlled ramp rate before an actual irradiance reduction occurs. However, such forecast-based techniques can lead to an increase in control complexity and necessitate additional sensing devices for forecasting. The accuracy of the predictions is also uncertain in practice. Hence, hardware-based strategies that utilize ESS are essential to deliver a reliable performance [12], [13].

A recent report in [14] indicates that batteries have emerged as an attractive candidate for utility-scale storage due to their high density, modularity, and decreasing cost projection trend. Although various ESS technologies have been utilized to mitigate the PV power fluctuations. These include but not limited to batteries [15], [16], [17], [18], capacitors [19], fuel cells [20], and hydrogen storage [21]. Hybrid ESSs that combine different storage technologies, such as battery with SC [22] and battery with hydrogen storage [23], have also been proposed to address the intermittent nature of PV power generation.

Majority of existing hardware-based PV power smoothing controls rely on filtering techniques primarily due to their ease of implementation and low computational effort [24]. Mitigating the PV power fluctuations with ESS is normally accomplished by using a well-known MAF [16], [17], [18], [19]. The ESS compensates for the difference between the instantaneous PV power and the averaged PV power, i.e., the difference between the input and the output of the MAF. After smoothing the PV power fluctuations, the procedure to restore the SoC of the ESS in [16], [17] is not elaborated. To avoid ESS capacity saturation, [18] regulates the SoC during the off-peak period, for instance, restoring the ESS at night from the grid to take advantage of time-of-use electricity price. Meanwhile, [19] adds the ESS voltage feedback to the MAF to maintain the stored energy after smoothing out the PV power. Although the MAF straightforwardly reduces the PV power fluctuations, its smoothing effectiveness interrelates with the degree of ESS utilization. A longer MAF averaging window length improves the PV power smoothness; however, it causes a prolonged ESS operation and, in turn, requires a larger ESS capacity, even when the PV power fluctuation is moderate. Such excessive operation degrades the ESS lifetime [25]. Conversely, a shorter MAF window length improves the ESS utilization at the expense of degraded PV power smoothness. To improve the memory effect (length of the averaging window) compromise of the traditional MAF, and improve the ESS utilization, [15] proposes an adaptive MAF algorithm that adjusts the averaging window length depending on the severity of the PV power fluctuations. The SoC variation is considered through a droop control in [15], but it does not ensure returning the SoC to its reference at the end of the day, which assumes the ESS capacity to be substantial enough to prevent saturation. A similar adaptive power smoothing approach with a hybrid ESS has been proposed in [26], which further enhances the adaptive MAF based on irradiance predictions. However, it has the drawbacks of increased computational burden and control complexities. Besides the MAF, other power smoothing filtering techniques, such as moving regression, double moving average, and Gaussian filter, are also explored in [27]. Nonetheless, filtering-based controls generally tend to exhibit oversmoothing due to the induced memory effect, resulting in oversizing the capacity and deteriorating the operational lifetime of the ESS [24].

To alleviate the ESS usage, a PRRC is introduced as an alternative approach for PV power smoothing applications in [11], [24], [28], [29], [30], [31]. The PRRC estimates the instantaneous PV power fluctuations by measuring the PV power difference over the sampling time period. This eliminates the memory effect and the ESS is only operated when necessary for mitigation. Even so, the capacity of ESS needs to be large enough to prevent saturation as the PRRC charges/discharges the ESS with a linear ramp rate [28], [29]. Hence, the PRRC in [30] and [31] adaptively varies the ramp rate of the PV power injected into the grid depending on the remaining ESS capacity. For instance, if the ESS SoC is high during discharge, the ramp rate will be small and vice versa. Similar considerations are also made for the charging scenario. Nevertheless, the SoC restoration strategy is overlooked in [30] and [31]. To reduce the ESS capacity

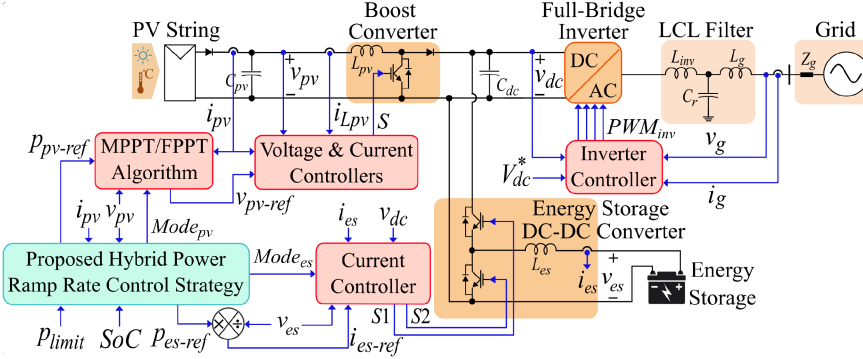


Fig. 1. Proposed hybrid PRRC implemented in a PV system with ESS.

requirement in PRRC, the control in [11] charges/discharges the ESS in advance by predicting the irradiance transients, which naturally regulates the SoC during the control process. However, this approach requires sensing equipment and the control reliability is affected by uncertainties in the predictions. Nonetheless, the ESS utilization in power smoothing applications is improved with PRRC as compared to the MAF.

All in all, conventional ESS-based power smoothing control schemes mentioned in the literature operate the PV system with MPPT, and as a result, ESS is required to mitigate both positive and negative irradiance transients. This necessitates reserving certain ESS capacity (ideally half the capacity) to cope with positive irradiance transients, which in turn, increases the required ESS capacity in PRRC. Moreover, the SoC should be effectively restored after mitigating the PV power fluctuations to avoid ESS saturation, viz., oversizing the ESS capacity.

This article proposes a hybrid PRRC strategy that effectively reduces the ESS utilization and capacity requirement by leveraging control flexibilities. Specifically, an advanced FPPT algorithm substitutes the ESS for controlling the PV power increasing rate, and therefore, the ESS is only required for negative irradiance transient events. Furthermore, the proposed strategy rapidly restores the SoC while respecting the power ramp rate limits. Considering the small ESS capacity, this rapid SoC restoration is critical for effectively responding to any subsequent events. A challenge in the proposed strategy is to ensure smooth control operation transitions between the PV system (i.e., MPPT and FPPT) and the ESS (i.e., charging, discharging, and standby), which is achieved by adopting a variable PV voltage-step to dynamically adjust the PV power.

The rest of this article is organized as follows. Section II introduces the proposed PRRC strategy. Section III presents some simulation results, and Section IV validates the proposed control effectiveness with experimental results. Simulation case studies to evaluate the effectiveness of the proposed hybrid control in reducing the required ESS capacity are provided in Section V. Finally, Section VI concludes the article.

II. PROPOSED PRRC STRATEGY

Fig. 1 shows a grid-connected PV system with an ESS connected to the dc-link. The inverter regulates the dc-link voltage

v_{dc} and injects the PV power to the ac grid. The proposed hybrid control outputs are as follows.

- 1) The PV power reference $p_{pv\text{-ref}}$.
- 2) The ESS power reference $p_{es\text{-ref}}$.
- 3) The PV operation mode (MPPT when $\text{Mode}_{pv} = 0$ and FPPT when $\text{Mode}_{pv} = 1$).
- 4) The ESS operation mode (ESS is in standby when $\text{Mode}_{es} = 0$ and active when $\text{Mode}_{es} = 1$).

Fig. 2 illustrates how these power references and operation modes are determined. The ramp rate of PV power variation $R(t)$ is measured as follows [7]:

$$R(t) = \frac{p_{pv}(t) - p_{pv}(t-T)}{T} \quad (1)$$

where $p_{pv}(t)$ denotes the measured PV power and T is the sampling period. The user-defined ramp rate limit R_{limit} should be large enough to prevent the control reacting to noises and MPPT operation [32].

The proposed algorithm engages by either an increase in irradiance event [$R(t) > R_{\text{limit}}$] or a decreasing one [$R(t) < -R_{\text{limit}}$], as shown in Fig. 2(a)–(d), respectively. As an example, R_{limit} is defined to be 10% of the rated PV power per minute in the Germany grid code [3]. While the proposed control remains engaged, Mode_{pv} and Mode_{es} retain their status until a trigger in the algorithm updates their value. Once the disengagement criteria [$p_{pv\text{-ref}}(k) = 0$ and $p_{es\text{-ref}}(k) = 0$] is met [see Fig. 2(a)], the ESS remains inactive and the PV system operates with MPPT for maximum generation.

A. Negative Slope Irradiance Transient [see Fig. 2(b)]

In the case of $R(t) < -R_{\text{limit}}$, the algorithm keeps Mode_{pv} at 0 for maximum PV power generation and activates the ESS ($\text{Mode}_{es} = 1$) to ensure the total power ramp rate limit. As the MPPT mechanism tracks the MPP by perturbing the PV voltage [32], its operation does not need $p_{pv\text{-ref}}$, and hence, $p_{pv\text{-ref}}(k)$ is set to 0. The total power injected into the grid $p_{\text{total}}(k)$ is decreased with a defined ramp rate [$p_{\text{total}}(k) = p_{\text{total}}(k-1) - P_{\text{limit}}$, wherein $P_{\text{limit}} = R_{\text{limit}}T$] by discharging the ESS according to $p_{es\text{-ref}}(k) = p_{\text{total}}(k) - p_{pv}(k)$. Accordingly, during the negative irradiance transient event, the computed $p_{es\text{-ref}}(k)$ increases and then, gradually decreases back to 0 after the

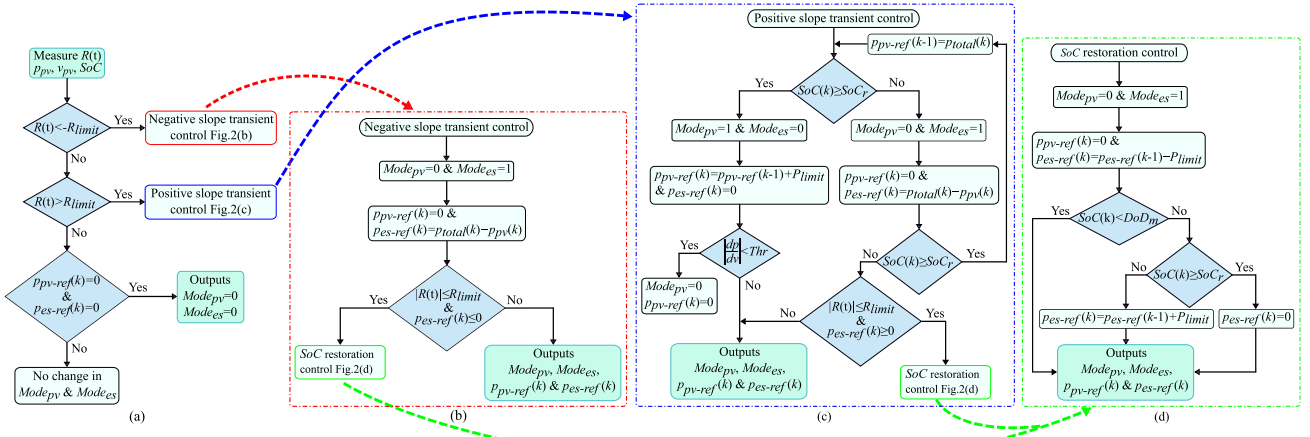


Fig. 2. Flowchart of the proposed hybrid PRRC strategy. (a) Control initialization based on PV power fluctuations. (b) Negative slope irradiance transient control. (c) Positive slope irradiance transient control. (d) ESS SoC restoration control.

irradiance transient settles [it can be observed from $t = 150$ s to $t = 265$ s in Fig. 4(a)]. This causes the ESS SoC to deviate away from its reference SoC_r (which can be 100% as the ESS is allowed to fully charge with the proposed strategy). The smoothing process completes when $p_{es-ref}(k) \leq 0$ and $|R(t)| \leq R_{limit}$. Subsequently, the proposed PRRC restores the SoC to SoC_r without violating the defined ramp rate, as shown in Fig. 2(d). To achieve this, the midpoint of depth-of-discharge

$$DoD_m = (SoC_r + SoC(j))/2 \quad (2)$$

is calculated at the instant j where p_{es-ref} crosses 0. Note that, when p_{es-ref} crosses 0, the SoC is at its minimum value. Then, the proposed control continues to generate negative $p_{es-ref}(k)$ to charge the ESS by ramping down p_{total} with R_{limit} until the SoC reaches DoD_m . Afterward, p_{total} is increased in a symmetrical way to converge back to p_{pv_max} by updating $p_{es-ref}(k) = p_{es-ref}(k-1) + P_{limit}$, as shown in Fig. 2(d). Once the ESS is fully restored, the proposed PRRC deactivates the ESS by updating $Mode_{es}$ to 0.

B. Positive Slope Irradiance Transient [See Fig. 2(c)]

If the SoC is full, only $Mode_{pv} = 1$ is updated to mitigate the positive slope power variation with the PV system using FPPT, as shown in Fig. 2(c). The proposed control then generates $p_{pv-ref}(k)$ for the FPPT as $p_{pv-ref}(k-1) + P_{limit}$ to gradually increase the PV power. Here, the initial value of $p_{pv-ref}(k-1)$ is the measured p_{pv} when the power fluctuation is detected. Since the slope of the P-V curve dp/dv at the MPP is close to zero (see Fig. 3), the proposed control compares the absolute value of dp/dv to a threshold to identify whether the PV operation is near the MPP. If it is true, the proposed control switches $Mode_{pv}$ to 0 for MPPT operation and resets p_{pv-ref} .

If $R(t)$ exceeds R_{limit} while the ESS is active (either to regulate p_{total} from a previous transient or restore the SoC), $Mode_{pv}$ and $Mode_{es}$ are kept unchanged. Then, the ESS steers p_{total} toward p_{pv} , i.e., $p_{total}(k)$ is decreased with R_{limit} rate if $p_{total}(k)$ is larger than $p_{pv}(k)$ and vice versa, as shown in Fig. 2(c). Thereafter,

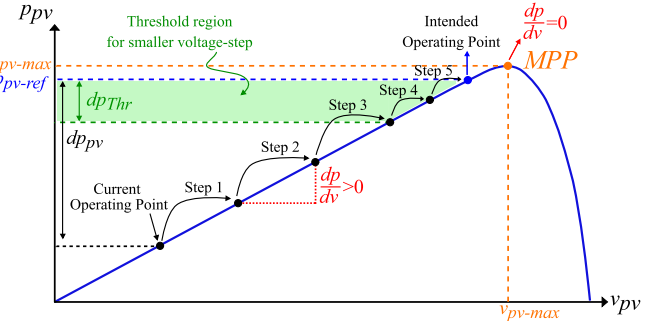


Fig. 3. Illustration of FPPT with a variable PV voltage-step size.

there are two possible scenarios in the following that can take place depending on the SoC level.

- The smoothing process completes when $p_{total}(k) = p_{pv}(k)$, and $R(t)$ is within the limits. In that case, the proposed control activates the SoC restoration mechanism, as illustrated in Fig. 2(d).
- While the smoothing process is in progress, the SoC reaches to SoC_r . To maintain the course of p_{total} with R_{limit} toward the PV MP p_{pv_max} , the PV operation switches to FPPT by updating $Mode_{pv}$ to 1 and the initial $p_{pv-ref}(k-1)$ is $p_{total}(k)$, as shown in Fig. 2(c). Afterward, the proposed control deactivates the ESS ($Mode_{es} = 0$) and resets p_{es-ref} . When $p_{total}(k)$ reaches p_{pv_max} , the PV system operates with MPPT ($Mode_{pv} = 0$).

C. Overall Control

To dynamically track p_{pv-ref} generated by the proposed PRRC and facilitate smooth PV control transitions, an FPPT [33] algorithm with variable PV voltage-step is implemented, as shown in Fig. 3. If the difference between p_{pv_ref} and p_{pv} is greater than a defined threshold ($dp_{pv} > dp_{Thr}$), a larger PV voltage-step V_{step} is used (which corresponds to Steps 1 – 3); otherwise, a smaller

TABLE I
SIMULATION PARAMETERS

Parameters	Values
PV maximum power*, $P_{pv\text{-max}}$	3 kW
PV maximum power point voltage*, V_{mpp}	400 V
DC-link voltage, V_{dc}	450 V
PV voltage-step, V_{step}	Large : 8 V Small : 1.5 V
Threshold of dp_{pv} , dp_{Thr}	50 W
Threshold of dp/dv , Thr	2 W/V
DC-DC converter switching frequency, f_{sw}	25 kHz
SC-based ESS, C_{es}	200 F
SC rated voltage, $V_{es\text{-rated}}$	25 V
Ramp rate limit, R_{limit}	10 W/s
Ramp rate sampling period, T	0.02 s
SoC reference, SoC_r	100 %

*Irradiance = 1000 W/m² and cell temperature = 25 °C

V_{step} is applied (which corresponds to Steps 4 and 5). The proposed control also restricts the FPPT operation to the left-hand side of the MPP to attain low power oscillation in steady-state while the transient dynamic performance is achieved with a variable V_{step} . Accordingly, the FPPT algorithm computes the voltage reference for the PV voltage controller, which in turn generates the reference for the current controller, as shown in Fig. 1. Then, the switching signal of the boost converter is generated by the PV current controller. The switching signals of the ESS converter, $S1$ and $S2$, are also generated according to $i_{es\text{-ref}} = p_{es\text{-ref}}/v_{es}$ by using a direct model predictive current control (see Fig. 1). The detailed implementation of current and voltage controllers is elaborated in [34]. The ESS converter switches as long as $Mode_{es} = 1$, otherwise, it remains in standby mode to reduce losses.

III. SIMULATION RESULTS

Simulations are performed in MATLAB/Simulink to verify the effectiveness and claims of the proposed hybrid PRRC strategy for a 3 – kW PV system with ESS. In the simulation, SC-based ESS is considered and its SoC value is estimated as [35]

$$SoC(k) = \frac{v_{es}(k)}{V_{es\text{-rated}}^2} \times 100\% \quad (3)$$

where $v_{es}(k)$ is the measured SC voltage at sampling instance k , and $V_{es\text{-rated}}$ is the SC rated voltage. Table I provides the simulation parameters, and Fig. 4 shows the simulation results of the proposed control under irradiance variations at different rates. The initial irradiance is stable at 0.6 kW/m² where the PV system is operating with MPPT ($Mode_{pv} = 0$) and the ESS is inactive ($Mode_{es} = 0$) as the SC is fully charged. At $t = 10$ s, the irradiance sharply increases to 1.0 kW/m², which causes $p_{pv\text{-max}}$ to increase from 1.85 to 3 kW with approximately 58 W/s, exceeding the allowable limit $R_{limit} = 10$ W/s, as can

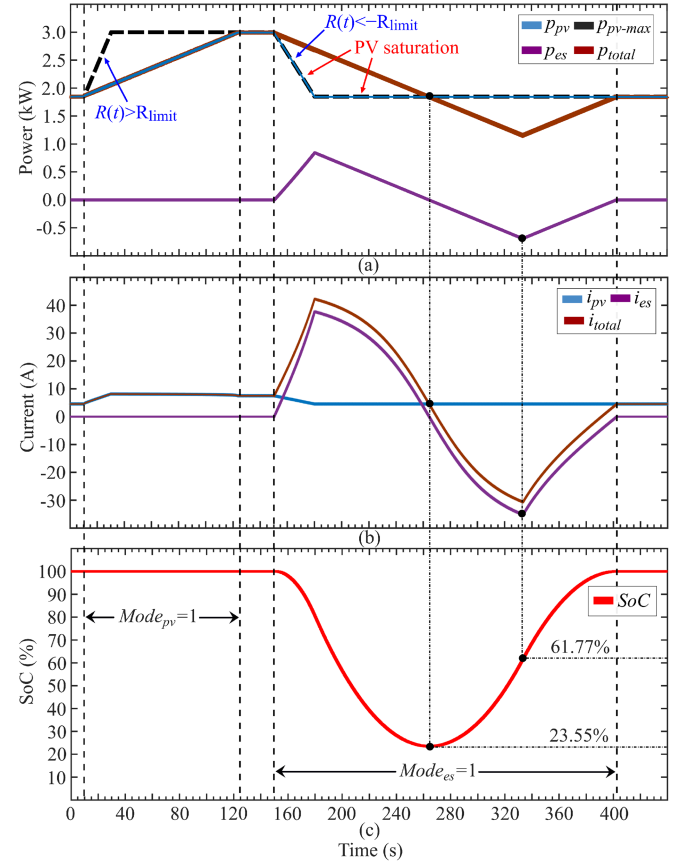


Fig. 4. Simulation results of the proposed control strategy under fast and slow irradiance fluctuations. (a) PV power, PV MP, SC-based ESS power, and total power. (b) PV current, SC current, and total current. (c) SC SoC.

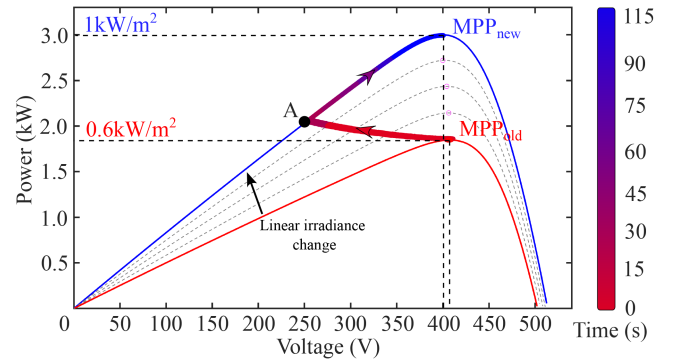


Fig. 5. Performance of the proposed PRRC exploiting FPPT for a positive slope irradiance fluctuation.

be seen in Fig. 4(a). Upon detecting the ramp limit violation, the proposed control switches the PV operation to FPPT ($Mode_{pv} = 1$) and steadily increases the PV power p_{pv} at permitted R_{limit} rate, which converges to $p_{pv\text{-max}}$ at approximately $t = 125$ s. Then, the proposed control updates the PV operation back to MPPT ($Mode_{pv} = 0$). During this increase in irradiance transient event, the ESS remains in standby mode [$i_{es} = 0$, as shown in Fig. 4(b)] as the PV power increment is effectively controlled with the PV software (i.e., $MPP_{old} \rightarrow A \rightarrow MPP_{new}$ in Fig. 5).



Fig. 6. Experimental hardware setup of the PV system with ESS.

Subsequently, the PV power deceleration with around 38 W/s is simulated at $t = 150$ s by decreasing the irradiance back to 0.6 kW/m². As the PV system saturates at the MP, as shown in Fig. 4(a), the proposed control regulates the total power p_{total} reduction by activating the ESS ($\text{Mode}_{\text{es}} = 1$) for power compensation. The smoothing process completes when p_{total} reaches new $p_{\text{pv-max}}$, i.e., $p_{\text{es}} = 0$, at approximately $t = 265$ s. At that instant, the proposed control calculates $\text{DoD}_m = 61.77\%$ based on the remaining SoC (23.55%) and its reference SoC_r (100%). The SC SoC is then restored by further decreasing p_{total} at the rate of R_{limit} until it reaches DoD_m where the ramp direction of p_{total} is reversed toward $p_{\text{pv-max}}$. The ESS is deactivated once the SC fully restores ($\text{Mode}_{\text{es}} = 0$).

It can be observed that the SoC value after mitigating the negative slope irradiance transient is 23.55% (i.e., SoC swing is more than 75%), as shown in Fig. 4(c). This indicates that this storage capacity would not be sufficient if a conventional PRRC technique [19], where a certain capacity is reserved, is used. For instance, if half of the capacity is reserved for positive slope irradiance transients, the conventional approach would require at least 60% more storage capacity in order to effectively regulate the negative slope PV power variation (note that this number is specific to this example and will vary according to PV power fluctuation rate and the PV capacity). Therefore, the simulation demonstrates the capability of the proposed method to reduce the ESS capacity, and thus the PV system footprint.

IV. EXPERIMENTAL RESULTS

The transient performance of the proposed PRRC strategy is validated experimentally by considering worst case scenarios where irradiance changes rapidly. The experimental test rig is shown in Fig. 6, where the PV module is emulated with a Chroma 61250-600S controllable dc source, switching signals for the dc-dc converters are generated by an Imperix B-Box controller, and a Cinergia (GE&EL+ vAC/DC) grid emulator is used as a grid-interfacing inverter that regulates the dc-link voltage. Table II provides the experimental parameters. BESS is used

TABLE II
EXPERIMENTAL PARAMETERS

Parameters	Values
PV MP*, $P_{\text{pv-max}}$	200 W
PV maximum power point voltage*, V_{mpp}	50 V
DC-link voltage, V_{dc}	100 V
PV voltage-step, V_{step}	Large : 4.5 V Small : 0.25 V
Threshold of dp_{pv} , dP_{Thr}	10 W
Threshold of dp/dv , Thr	2 W/V
Sampling frequency of PV system, f_{pv}	100 Hz
PV-side capacitor, C_{pv}	0.5 mF
PV dc-dc converter inductance, L_{pv}	4.72 mH
ESS dc-dc converter inductance, L_{es}	4.72 mH
DC-DC converter switching frequency, f_{sw}	25 kHz
Battery rated capacity, E_{es}	336 Wh
Battery rated voltage, $V_{\text{es-rated}}$	48 V
Ramp rate limit, R_{limit}	10 W/s
Ramp rate sampling period, T	0.02 s
SoC reference, SoC_r	100 %

*Irradiance = 1000 W/m² and cell temperature = 25 °C

in the experiments and its SoC value is estimated using a simple Coulomb counting approach as follows [36]:

$$\text{SoC}(k) = \text{SoC}(k-1) - \int_{(k-1)T}^{kT} (i_{\text{es}}/E_{\text{es}}) dt \quad (4)$$

where i_{es} and E_{es} are the BESS current and rated capacity, respectively.

A. PRRC Operation Under Rapid Irradiance Transients

The initial irradiance is emulated to be constant at 0.5 kW/m², and accordingly, the PV system is extracting the MP 100 W using MPPT ($\text{Mode}_{\text{pv}} = 0$) and the ESS is inactive ($\text{Mode}_{\text{es}} = 0$) as the battery is full (SoC = 100%), as shown in Fig. 7. A rapid increase in irradiance from 0.5 to 1 kW/m² is emulated at approximately $t = 17$ s, which causes the PV power p_{pv} to fluctuate beyond the allowed ramp rate R_{limit} . Since the PV power change is positive and the BESS is fully charged, the proposed PRRC only switches the PV operation to FPPT to regulate the PV power increment at the allowed ramp rate while the BESS remains in standby mode, i.e., $p_{\text{total}} = p_{\text{pv}}$. As the ramp rate limit of p_{total} in the experimentation is defined to be 10 W/s, p_{pv} reaches the PV MP $p_{\text{pv-max}} = 200$ W at approximately $t = 27$ s. The proposed control switches Mode_{pv} back to 0 when dp/dv becomes smaller than its threshold (PV operation is close to the MPP) to continue the PV power extraction with MPPT, as shown in Fig. 7(b). Then, another rapid PV power change is emulated again by reducing the irradiance to 0.5 kW/m² at approximately $t = 45$ s. Here, the FPPT becomes ineffective as the PV operation becomes saturated at the MP, unlike the previous increase in irradiance transient case.

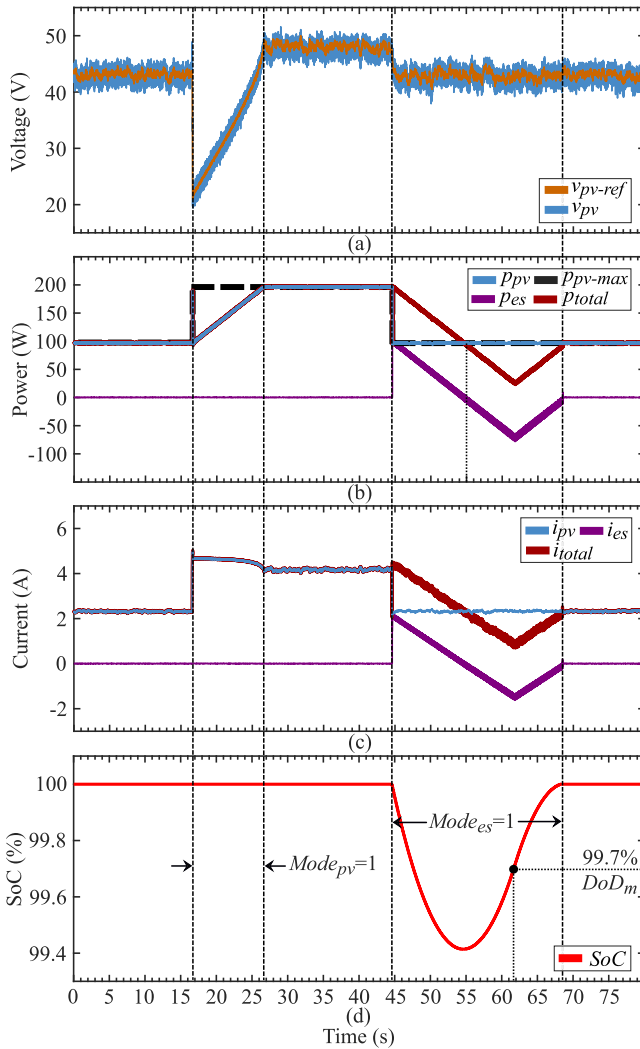


Fig. 7. Experimental investigation of the proposed control strategy under rapid irradiance transients. (a) PV voltage, and PV voltage reference. (b) PV power, PV MP, BESS power, and total power. (c) PV current, battery current, and total current. (d) Battery SoC.

Therefore, the proposed PRRC keeps $Mode_{pv} = 0$ to minimize the BESS discharge by maximizing the PV power generation, and simultaneously, activates the BESS ($Mode_{es} = 1$) to regulate the deceleration rate of the total power to $-R_{\text{limit}}$, i.e., $p_{\text{total}} = p_{\text{pv_max}} + p_{\text{es}}$. The controlled p_{total} ramping down event concludes when p_{es} becomes zero at around $t = 55$ s. Before switching off the BESS, the battery SoC needs to be restored to effectively respond to any subsequent irradiance reduction transients. Hence, to initiate the SoC restoration procedure, the proposed PRRC calculates $\text{DoD}_m = 99.7\%$ and until the SoC reaches DoD_m , the BESS charging power grows, which in turn, further decreases p_{total} below $p_{\text{pv_max}}$ with R_{limit} rate of change, as can be seen in Fig. 7(b) and 7(c). One can observe in Fig. 7(d) that the SoC profile becomes more inclined as p_{es} increases. This growing BESS charging power is reduced back when the SoC reaches DoD_m at approximately $t = 62$ s to converge p_{total} back to $p_{\text{pv_max}}$. Once the BESS capacity is fully restored, $Mode_{es}$ is

updated to 0 to put the BESS into standby mode and thereafter, p_{total} is equal to $p_{\text{pv_max}}$.

Fig. 7 results demonstrate that the proposed PRRC effectively deals with severe PV power fluctuations and transforms them into a smooth p_{total} varying with defined ramp rate, which is seen from the grid inverter perspective. Thanks to the FPPT with a variable voltage-step (see Fig. 3), the PV system is able to quickly track the PV power reference $p_{\text{pv_ref}}$, as can be observed in Fig. 7(a). The experimental results demonstrate that the battery SoC is fully restored without violating the ramp limit. Besides, the need to reserve certain BESS capacity for positive irradiance transients becomes avoidable with the proposed strategy and thus, the BESS capacity can be reduced.

B. PRRC Operation Under Multiple Irradiance Transients in the Same Direction

In practice, the solar irradiance can fluctuate successively depending on the density of passing cloud cover. Therefore, this section investigates the effectiveness of the proposed PRRC under an emulated environment with multiple rapid changes in irradiance, and the experimental results are shown in Fig. 8. Initially, the PV system is operating with the MPPT ($Mode_{pv} = 0$), the SoC is at 100% and the BESS is in standby ($Mode_{es} = 0$). Then, a rapid increase in irradiance from 0.5 kW/m^2 to 0.75 kW/m^2 at approximately $t = 17$ s causes a positive change in PV power. This triggers the proposed control to update $Mode_{pv}$ to 1, which initiates a gradual increase in p_{pv} with R_{limit} . Another positive irradiance change (from 0.75 to 1 kW/m^2) occurs at around $t = 21.5$ s right before the PV power smoothing process completes, as shown in Fig. 8(b). Since the PV power transient is positive, the BESS remains inactive, while the PV system accurately tracks its voltage reference $v_{\text{pv_ref}}$ at that instant (steadily increasing $v_{\text{pv_ref}}$ adaptively shifts from approximately 40 to 30 V, as shown in Fig. 8(a)) in order to maintain p_{pv} increment with 10 W/s . Eventually, the proposed control updates $Mode_{pv}$ back to 0 when the PV operation is near the MPP at approximately $t = 27$ s. Similar multiple rapid irradiance changes that decrease $p_{\text{pv_max}}$ from 200 to 150 W (at about $t = 42$ s) and to 100 W (at $t = 47.5$ s) are emulated. In this case, the proposed control maintains $Mode_{pv} = 0$ for MP generation and updates $Mode_{es} = 1$ to compensate the required power from the BESS for p_{total} ramping down smoothly at $-R_{\text{limit}}$ rate. As can be observed in Fig. 8(b), p_{es} gradually decreases as p_{total} approaches to p_{pv} in both transients. When the power smoothing completes, i.e., $p_{\text{es}} = 0$, the proposed control calculates $\text{DoD}_m = 99.85\%$ and restores the SoC by maintaining ramp-down course of p_{total} . The course of p_{total} is later changed to ramp-up once the SoC hits DoD_m at around $t = 57$ s by decreasing the ESS charging rate [see Fig. 8(c)], and the proposed control returns the BESS into standby mode ($Mode_{es} = 0$) after the SoC is fully restored at $t = 62$ s, as shown in Fig. 8(d).

At the instant of sudden irradiance changes, total power/current momentary transients can be observed, as shown in Fig. 8(b) and 8(c). This is in fact due to the sampling interval T adopted for $R(t)$ measurement in (1), which is the delay in the control response. This T should have a large enough

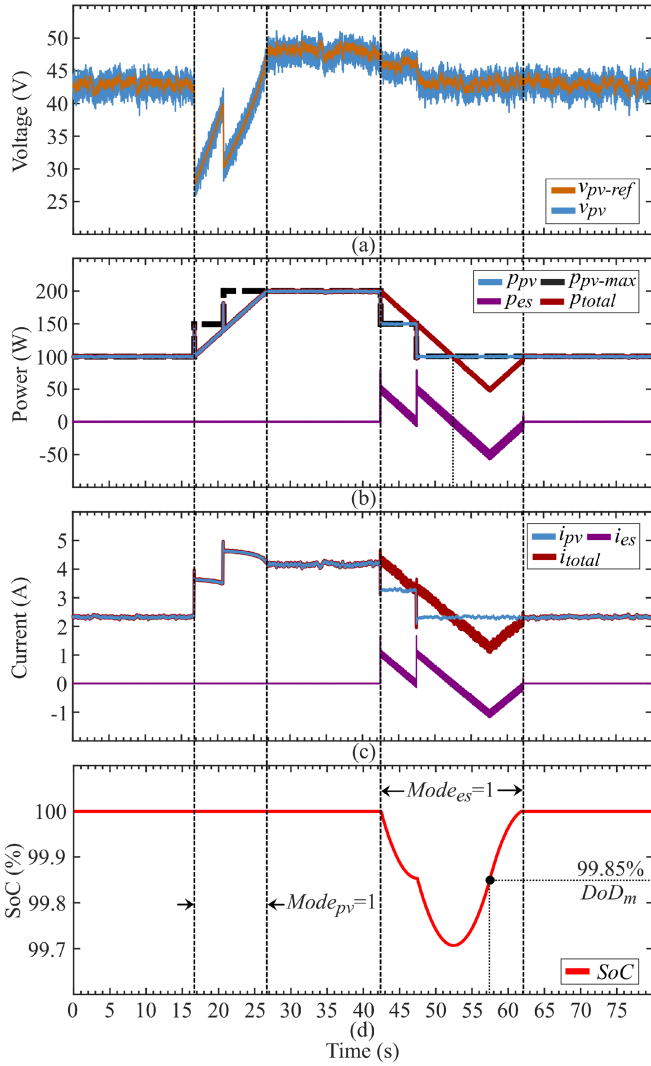


Fig. 8. Experimental validation of the proposed control strategy under multiple rapid irradiance transients. (a) PV voltage, and PV voltage reference. (b) PV power, PV MP, BESS power, and total power. (c) PV current, battery current, and total current. (d) Battery SoC.

value to allow a meaningful ramp rate measurement, while its value should be small enough to be negligible from the perspective of inverter capacitor voltage controller. Accordingly, the experimental results validate that the proposed PRRC effectively regulates power fluctuations by using a software-based flexible PV power control strategy for positive PV power fluctuations and a hardware-based BESS for negative PV power fluctuations.

C. PRRC Operation Under Consecutive Irradiance Transients

This section further analyzes multiple irradiance transients, in particular, how the proposed PRRC responds to a sudden increase in irradiance while the BESS is still in use. As shown in Fig. 9(b), the maximum PV power $p_{pv\text{-}max}$ decreases from 200 to 100 W due to a rapid decrease in irradiance at approximately $t = 16$ s. Accordingly, the proposed control activates the BESS (Mode_{es} = 1) and discharges the required p_{es} to maintain the

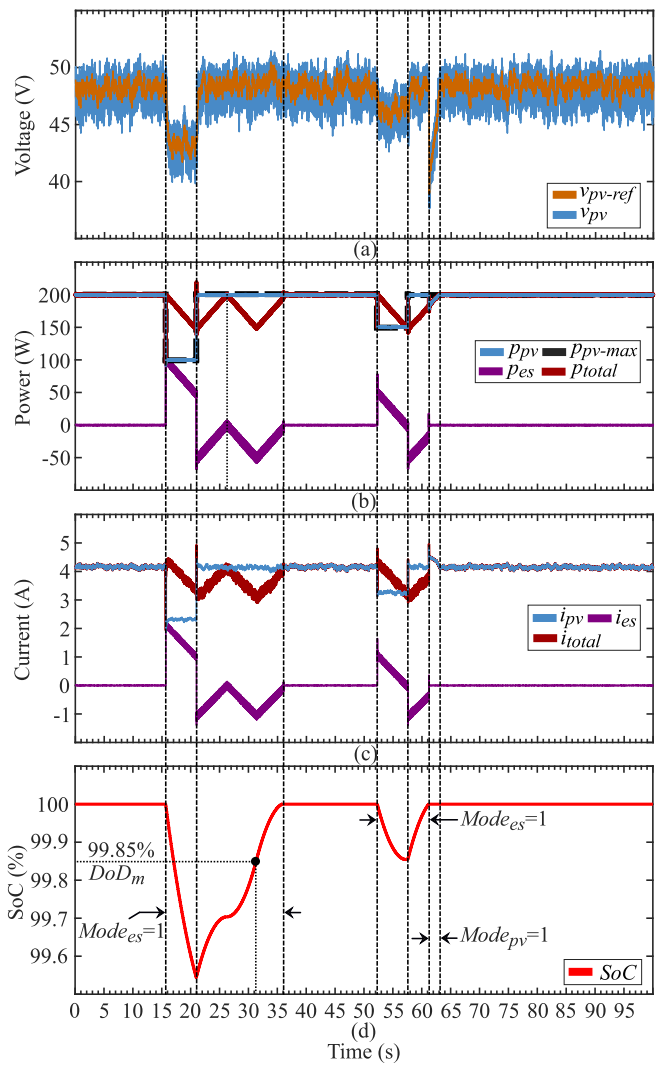


Fig. 9. Experimental results of the proposed PRRC charging the BESS under positive irradiance transients. (a) PV voltage, and PV voltage reference. (b) PV power, PV MP, BESS power, and total power. (c) PV current, battery current, and total current. (d) Battery SoC.

reduction rate of p_{total} at $-R_{\text{limit}}$. While p_{total} is decreasing with a controlled ramp rate, irradiance suddenly increases back to 1 kW/m^2 at $t = 21$ s, which makes $p_{pv\text{-}max}$ now greater than p_{total} . The proposed control correspondingly switches the ramp direction of p_{total} toward $p_{pv} = p_{pv\text{-}max}$ by controlling the BESS charging power p_{es} . At around $t = 26$ s, p_{total} reaches $p_{pv\text{-}max}$ although the SoC is not at its reference. The proposed control subsequently computes DoD_m = 99.85%, and decreases p_{total} with $-R_{\text{limit}}$ rate to continue the BESS charging process, as shown in Fig. 9(c). The regulated p_{total} is then converged back to $p_{pv\text{-}max}$ as soon as the SoC reaches DoD_m at around $t = 31$ s [see Fig. 9(b) and (d)], and the BESS becomes inactive (Mode_{es} = 0) at $t = 36$ s after the SoC is fully restored. Throughout this process, the PV system operates with MPPT (Mode = 0) to either minimize the BESS discharging power or maximize the BESS charging power. Likewise, the proposed control utilizes the BESS (Mode_{es} = 1) to regulate p_{total} reduction rate after detecting the negative irradiance change from 1 kW/m^2

at approximately $t = 52$ s. It charges back the BESS while controlling p_{total} increment with R_{limit} from $t = 57.5$ s onward where the irradiance rebounds to 1 kW/m^2 , as shown in Fig. 9(b). At around $t = 61$ s, the SoC has been fully restored, i.e., the BESS capacity is saturated [see Fig. 9(d)], however, the controlled p_{total} has not yet fully converged to $p_{\text{pv_max}}$. In this case, the proposed control disconnects the BESS ($\text{Mode}_{\text{es}} = 0$) to prevent overcharging and simultaneously operates the PV system with FPPT by updating Mode_{pv} to 1. The FPPT algorithm then dynamically adjusts the PV voltage, as shown in Fig. 9(a), to track $p_{\text{pv_ref}}$ generated by the proposed PRRC and maintain p_{total} ramp rate. The PV system continues to operate again with MPPT by switching Mode_{pv} back to 0 after p_{total} becomes $p_{\text{pv_max}}$ at about $t = 63$ s.

The experimental results show that the proposed PRRC effectively considers the SoC regulation and takes full advantage of the FPPT-based PV control strategy in order to improve the BESS utilization. As the BESS capacity is fully restored after mitigating the PV power fluctuations, the FPPT with a variable PV voltage-step is exploited under upward irradiance transients to prevent overcharging the BESS.

V. PERFORMANCE EVALUATION OF PRRC STRATEGIES

To further demonstrate the advantages of the work, the proposed hybrid PRRC and three conventional control algorithms are compared in terms of PV energy yield, BESS capacity and its utilization behavior. Specifically, the following PRRCs are considered, Strategy $s1$: FPPT-based PRRC [7], Strategy $s2$: FPPT with reserve power-based PRRC [9], Strategy $s3$: BESS-based PRRC [29], and Strategy $s4$: proposed hybrid PRRC. Both $s1$ and $s2$ are known to be cost-effective as they do not involve any hardware ESS for control, whereas $s3$ relies entirely on the BESS to mitigate PV power fluctuations.

The simulation analysis is carried out with a real-field one-day highly-fluctuated irradiance profile (with 1-min resolution) captured in Ontario, Canada [36]. In this simulated case study, the rated power of the PV system P_{rated} is considered to be 3 kW at solar irradiance 1 kW/m^2 , and the permitted R_{limit} is 5 W/s. Note that the BESS capacity is sized in such a way that 95% of the capacity is effectively utilized, while the remaining 5% serves as a safety margin. Fig. 10 presents the overall simulation results of the case study.

A. Cost-Effective Software-Based PRRCs

The simulation results for $s1$ are shown in Fig. 10(a) and (b). As long as the maximum PV power $p_{\text{pv_max}}$ fluctuations due to irradiance changes are positive, the Strategy $s1$ successfully regulates the PV power p_{pv} increasing rate at the allowed R_{limit} . However, the FPPT algorithm becomes saturated at the MPP when $p_{\text{pv_max}}$ rapidly decreases below the regulating p_{pv} due to negative irradiance changes [highlighted in green circles in Fig. 10(b)]. As Strategy $s1$ does not incorporate any ESS, the control becomes ineffective in regulating p_{pv} reduction rate and ends up generating $p_{\text{pv_max}}$ during negative irradiance transients.

In contrast, Strategy $s2$ reserves 20% of $p_{\text{pv_max}}$ (in this case study), upholding a virtually stored energy for negative irradiance changes. Fig. 10(g) [zoomed in on Fig. 10(f)] shows that Strategy $s2$ can regulate both positive and negative PV power changes at the defined R_{limit} with the help of the reserved power. This method is effective as long as the reserved PV power is sufficient to handle the negative PV power changes [highlighted in red circles in Fig. 10(g)]. However, if the PV power drop due to an abrupt irradiance reduction exceeds the reserved PV power [highlighted in green circles in Fig. 10(g)], the PV operation ends up at the MPP, similar to $s1$, and p_{pv} reduction rate becomes uncontrolled. Therefore, this simulation analysis demonstrates that while $s1$ and $s2$ are recognized as cost-effective solutions, they are not truly viable for effective PV power smoothing.

B. Hardware-Based PRRC

The simulation results for hardware BESS-based Strategy $s3$ is illustrated in Fig. 10(c)–(e). Strategy $s3$ operates the PV system with MPPT to extract the maximum PV energy yield at all times [i.e., $p_{\text{pv}} = p_{\text{pv_max}}$ in Fig. 10(c)]. Consequently, the BESS is heavily relied upon to regulate both positive and negative PV power fluctuations, necessitating the reservation of a portion of the BESS capacity (50% in this case study) to be able to cope with positive PV power transients. This behavior can be observed in Fig. 10(e) where the SoC regulation, after smoothing the PV power, is capped at 50%. Overall, Strategy $s3$ effectively smoothens the total injected power p_{total} fluctuations at R_{limit} by continuously operating the BESS, as shown in Fig. 10(d). However, continuous BESS utilization in highly intermittent irradiance environments, such as in this case study, leads to an accelerated degradation of its lifetime [25], [34].

C. Proposed Hybrid (Hardware/Software-Based) PRRC

The proposed hybrid PRRC (Strategy $s4$), as shown in Figs. 10(h)–(j), selectively operates the BESS during negative irradiance transients when the PV system reaches the MPP saturation. After smoothing the PV power, the SoC is fully restored to 100% [see Fig. 10(j)]. During positive irradiance transients, when the BESS is fully charged, the proposed hybrid control leverages the dynamic FPPT to gradually increase p_{total} at R_{limit} in a controlled manner [$p_{\text{total}} = p_{\text{pv}}$, highlighted in a red circle in Fig. 10(i)]. If the BESS is not fully restored during positive irradiance fluctuations, the PV system operates with MPPT, and the proposed control regulates p_{total} at R_{limit} by charging the BESS with surplus PV generation. Once the SoC is full, the PV operation switches to dynamic FPPT [highlighted in green circles in Fig. 10(i)].

D. Performance Comparison

Table III presents a comprehensive evaluation of the four PRRC strategies. The maximum energy yield of a 3 – kW PV system under a specific one-day irradiance profile [37] is 15.926 kWh, and Strategy $s3$ generation is the highest among all strategies. Strategies $s1$ and $s2$ curtail the total PV generation capacity by 26.89% and 38.28%, respectively, to regulate

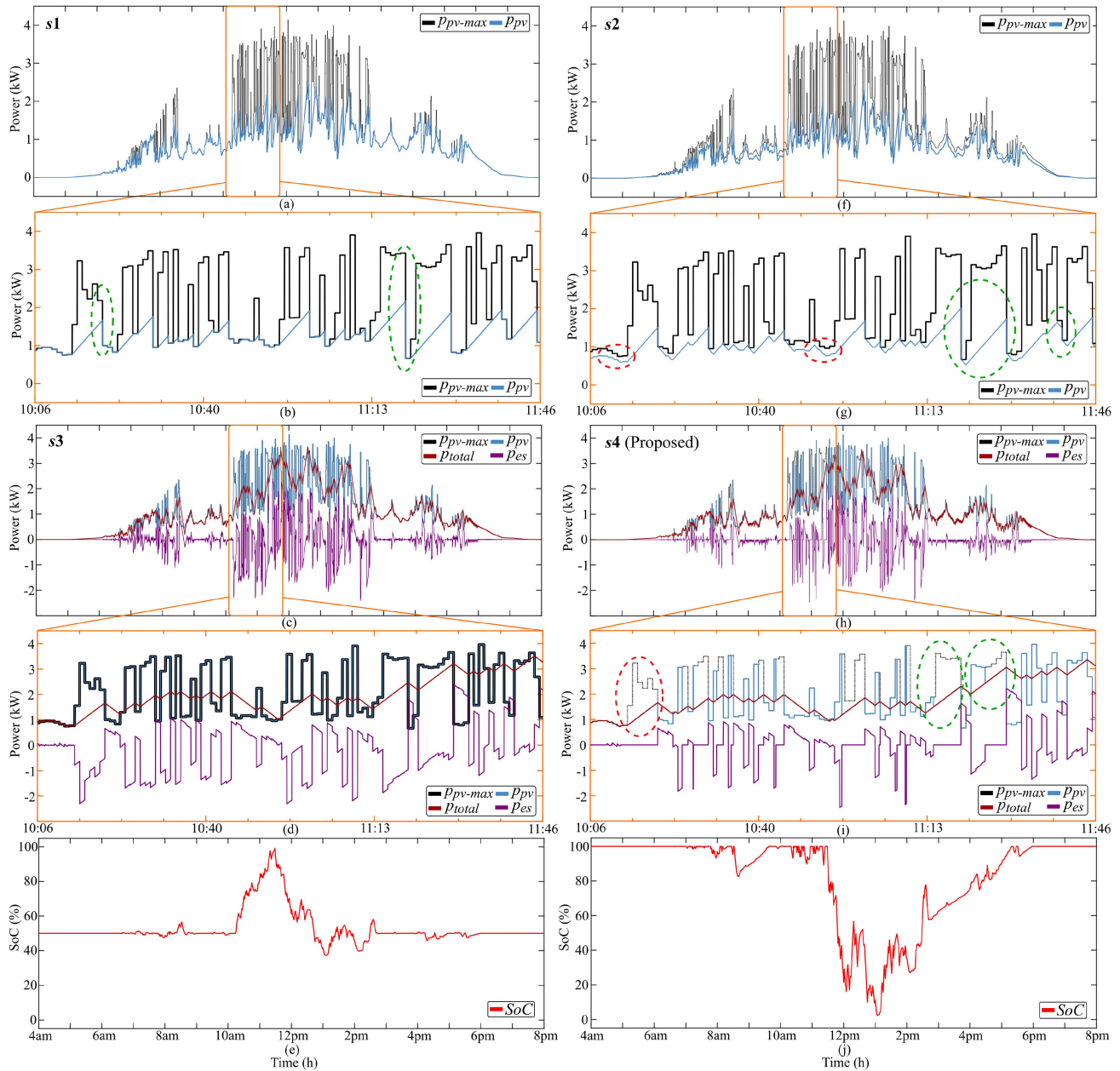


Fig. 10. Simulation results of the four PRRC strategies under a real-field one-day highly-fluctuated irradiance profile. *s1*: (a) PV MP, and PV power. (b) Zoomed in version of (a). *s3*: (c) PV MP, PV power, total injected power, and BESS power. (d) Zoomed in version of (c). (e) Battery SoC. *s2*: (f) PV MP, and PV power. (g) Zoomed in version of (f). *s4*: (h) PV MP, PV power, total injected power, and BESS power. (i) Zoomed in version of (h), and (j) battery SoC.

positive PV power fluctuations [here, the significant PV power curtailment has been done due to severe PV MP fluctuations, as can be seen in Fig. 10(b) and (g)]. Notably, Strategy *s2* exhibits more significant energy curtailment (resulting in the lowest energy yield) due to a continuous PV energy reservation. Furthermore, Strategy *s2* occasionally exceeds the allowed ramp limit during abrupt negative PV power transients, as explained in Section V-A. Thus, Strategy *s2* lacks economic attractiveness and practicality. The proposed Strategy *s4* also curtails a certain amount of PV energy (5.19%) compared to Strategy *s3* to control the positive PV power fluctuation rate with dynamic FPPT. However, in return, the proposed Strategy *s4* offers salient

advantages in terms of battery lifetime and the size, as the SoC can be fully restored to 100% and the BESS utilization is enhanced by operating it only during negative PV power fluctuations or the charging process. The proposed Strategy *s4* only requires 399 Wh energy storage capacity, whereas Strategy *s3* requires a capacity of 1109 Wh in this case study. The computational burden of all four strategies is also provided in Table III. It can be observed that Strategies *s3* and *s4* demand higher computational load compared to the software-based Strategies *s1* and *s2*. This is in fact due to the additional controller for the BESS management, which is an essential expense to ensure a reliable PRRC during negative irradiance transients.

TABLE III
COMPARISON OF FOUR PRRC STRATEGIES OVER ONE DAY SIMULATION

	<i>s</i> 1 [7]	<i>s</i> 2 [9]	<i>s</i> 3 [29]	<i>s</i> 4 (Proposed)
Energy yield (kWh)	11.643	9.83	15.926	15.098
Energy curtailed (%)	26.89	38.28	0	5.19
Ramp Up Violations	0	0	0	0
Ramp Down Violations	Yes	Occasionally	0	0
Battery Capacity* (Wh)	NA	NA	1109	399
Final SoC (%)	NA	NA	50	100
Computational Load† (%)	14.3	14.3	20.8	21.3
Maximum PV energy yield:	15.926 kWh			

*Battery capacity sizing is based on 95 % utilization with reserving 5 % as a safety margin.

†Each strategy is loaded to an Imperix B-Box controller to quantify the central processing unit (CPU) usage at 50 kHz sampling rate.

On the whole, both Strategies *s*3 and *s*4 achieve effective PV power smoothing, but at the cost of the BESS and the higher computational load. Although the proposed Strategy *s*4 results in a 5.19% reduction in PV energy production and a 0.5% increment in CPU occupancy compared to Strategy *s*3, it enhances the BESS utilization by alleviating extended operation periods. The proposed control also significantly reduces the required BESS capacity by 64%, from 1109 to 399 Wh. This specific percentage will vary depending on the weather profile.

In the future, the feasibility of the proposed hybrid PRRC will be further verified through economic analysis, which includes generation and installation cost, efficiency and lifetime of the PV system and the BESS, and the PV power curtailment.

VI. CONCLUSION

An ESS-based PV PRRC strategy has been proposed in this article, which reduces the required ESS capacity in PV power smoothing applications by employing an FPPT algorithm to deal with positive irradiance transients. The ESS is utilized only when the PV operation saturates at the MPP under negative irradiance transients. The proposed control rapidly restores the ESS SoC to full after regulating the PV power intermittency. This stands in contrast with conventional control approaches where the ESS SoC is kept as low as 50%. The experimental results attest that the proposed control performs a smooth transition between PV and ESS control operations under rapid irradiance transients, and effectively enforces a defined ramp rate to the total power variations. Furthermore, computational burden analysis and simulation case studies with a specific real-field one-day highly fluctuated irradiance profile are also presented. The proposed hybrid approach reduced the PV generation by only 5.19% and increased the computational burden by merely 0.5% to yield a substantial 64% reduction in the required BESS capacity compared to the conventional ESS-based solution.

REFERENCES

- [1] REN21, “Renewables 2023 global status report,” 2023. [Online]. Available: <https://www.ren21.net/gsr-2023/>
- [2] M. Karimi, H. Mokhlis, K. Naidu, S. Uddin, and A. Bakar, “Photovoltaic penetration issues and impacts in distribution network—A review,” *Renewable Sustain. Energy Rev.*, vol. 53, pp. 594–605, Jan. 2016.
- [3] BDEW, “Technical guideline generating plants connected to the medium voltage network,” Dec. 2008. [Online]. Available: <https://erranet.org/download/generating-plants-connected-to-medium-voltage-network/>
- [4] Eur. Netw. of Transmiss. Syst. Operators for Electricity, “Network code for requirements for grid connection applicable to all generators,” Tech. Rep. Mar. 2013. [Online]. Available: <https://www.entsoe.eu.2013>
- [5] Danish Grid Codes, “Technical regulation 3.2.2 for PV power plants with a power output above 11 kW,” Jun. 2016. [Online]. Available: https://en.energinet.dk/media/evsjqt/technical-regulation-3_2_2-for-pv-power-plants-above-11-kw.pdf
- [6] G. C. Mahato, S. R. Biswal, T. R. Choudhury, B. Nayak, and S. B. Santra, “Review of active power control techniques considering the impact of MPPT and FPPT during high PV penetration,” *Sol. Energy*, vol. 251, pp. 404–419, Feb. 2023.
- [7] A. Sangwongwanich, Y. Yang, and F. Blaabjerg, “A cost-effective power ramp-rate control strategy for single-phase two-stage grid-connected photovoltaic systems,” in *Proc. IEEE Energy Convers. Congr. Expo.*, 2016, pp. 1–7.
- [8] M. Haghigheh, M. Niroomand, and H. D. Tafti, “An adaptive power ramp rate control method for photovoltaic systems,” *IEEE J. Photovolt.*, vol. 12, no. 2, pp. 557–564, Mar. 2022.
- [9] X. Li, H. Wen, B. Chen, S. Ding, and W. Xiao, “A cost-effective power ramp rate control strategy based on flexible power point tracking for photovoltaic system,” *Sol. Energy*, vol. 208, pp. 1058–1067, Sep. 2020.
- [10] A. Narang et al., “Dynamic reserve power point tracking in grid-connected photovoltaic power plants,” *IEEE Trans. Power Electron.*, vol. 38, no. 5, pp. 5939–5951, May 2023.
- [11] X. Chen, Y. Du, H. Wen, L. Jiang, and W. Xiao, “Forecasting-based power ramp-rate control strategies for utility-scale PV systems,” *IEEE Trans. Ind. Electron.*, vol. 66, no. 3, pp. 1862–1871, Mar. 2019.
- [12] S. Sukumar, S. Mekhilef, H. Mokhlis, and M. Karimi, “Mitigating methods of power fluctuation of photovoltaic (PV) sources—A review,” *Renewable Sustain. Energy Rev.*, vol. 59, pp. 1170–1184, Jun. 2016.
- [13] G. G. Farivar et al., “Grid-connected energy storage systems: State-of-the-art and emerging technologies,” in *Proc. IEEE*, vol. 111, no. 4, pp. 397–420, Apr. 2023.
- [14] NREL, “Cost projections for utility-scale battery storage: 2021 update,” 2023. [Online]. Available: <https://www.nrel.gov/docs/fy21osti/79236.pdf>
- [15] R. Kini, D. Raker, T. Stuart, R. Ellingson, M. Heben, and R. Khanna, “Mitigation of PV variability using adaptive moving average control,” *IEEE Trans. Sustain. Energy*, vol. 11, no. 4, pp. 2252–2262, Oct. 2020.
- [16] V. Rallabandi, O. M. Akeyo, N. Jewell, and D. M. Ionel, “Incorporating battery energy storage systems into multi-MW grid connected PV systems,” *IEEE Trans. Ind. Appl.*, vol. 55, no. 1, pp. 638–647, Jan./Feb. 2019.
- [17] O. M. Akeyo, V. Rallabandi, N. Jewell, and D. M. Ionel, “The design and analysis of large solar PV farm configurations with dc-connected battery systems,” *IEEE Trans. Ind. Appl.*, vol. 56, no. 3, pp. 2903–2912, May/Jun. 2020.
- [18] V. T. Tran, M. R. Islam, D. Sutanto, and K. M. Muttaqi, “Mitigation of solar PV intermittency using ramp-rate control of energy buffer unit,” *IEEE Trans. Energy Convers.*, vol. 34, no. 1, pp. 435–445, Mar. 2019.
- [19] N. Kakimoto, H. Satoh, S. Takayama, and K. Nakamura, “Ramp-rate control of photovoltaic generator with electric double-layer capacitor,” *IEEE Trans. Energy Convers.*, vol. 24, no. 2, pp. 465–473, Jun. 2009.
- [20] P. Prabhakaran and V. Agarwal, “Novel four-port DC-DC converter for interfacing solar PV-fuel cell hybrid sources with low-voltage bipolar DC microgrids,” *IEEE J. Emerg. Sel. Topics Power Electron.*, vol. 8, no. 2, pp. 1330–1340, Jun. 2020.
- [21] P. Garcia-Trivino, L. de Oliveira-Assis, E. P. P. Soares-Ramos, R. Sarrias-Mena, C. A. Garci-Vazquez, and L. M. Fernandez-Ramirez, “Supervisory control system for a grid-connected MVDC microgrid based on z-source converters with PV, battery storage, green hydrogen system and charging station of electric vehicles,” *IEEE Trans. Ind. Appl.*, vol. 59, no. 2, pp. 2650–2660, Mar. 2023.
- [22] M. K. Behera and L. C. Saikia, “A novel resilient control of grid-integrated solar PV-hybrid energy storage microgrid for power smoothing and pulse power load accommodation,” *IEEE Trans. Power Electron.*, vol. 38, pp. 3965–3980, Mar./Apr. 2023.

- [23] A. M. Abomazid, N. A. El-Taweel, and H. E. Z. Farag, "Optimal energy management of hydrogen energy facility using integrated battery energy storage and solar photovoltaic systems," *IEEE Trans. Sustain. Energy*, vol. 13, no. 3, pp. 1457–1468, Jul. 2022.
- [24] S. Sukumar, M. Marsadek, K. Agileswari, and H. Mokhlis, "Ramp-rate control smoothing methods to control output power fluctuations from solar photovoltaic (PV) sources - A review," *J. Energy Storage*, vol. 20, pp. 218–229, Dec. 2018.
- [25] H. W. Yan et al., "Battery lifetime extension in a stand-alone microgrid with flexible power point tracking of photovoltaic system," *IEEE J. Emerg. Sel. Topics Power Electron.*, vol. 11, no. 2, pp. 2281–2290, Apr. 2023.
- [26] A. A. Abdalla, M. S. E. Moursi, T. H. El-Fouly, and K. H. A. Hosani, "A novel adaptive power smoothing approach for PV power plant with hybrid energy storage system," *IEEE Trans. Sustain. Energy*, vol. 14, no. 3, pp. 1457–1473, Jul. 2023.
- [27] M. A. Syed and M. Khalid, "Moving regression filtering with battery state of charge feedback control for solar PV firming and ramp rate curtailment," *IEEE Access*, vol. 9, pp. 13198–13211, Jan. 2021.
- [28] D. S. Kumar, S. Maharjan, Albert, and D. Srinivasan, "Ramp-rate limiting strategies to alleviate the impact of PV power ramping on voltage fluctuations using energy storage systems," *Sol. Energy*, vol. 234, pp. 377–386, Mar. 2022.
- [29] X. Li, D. Hui, and X. Lai, "Battery energy storage station (BESS)-based smoothing control of photovoltaic (PV) and wind power generation fluctuations," *IEEE Trans. Sustain. Energy*, vol. 4, no. 2, pp. 464–473, Apr. 2013.
- [30] M. J. E. Alam, K. M. Muttaqi, and D. Sutanto, "A novel approach for ramp-rate control of solar PV using energy storage to mitigate output fluctuations caused by cloud passing," *IEEE Trans. Energy Convers.*, vol. 29, no. 2, pp. 507–518, Jun. 2014.
- [31] I. de la Parra, J. Marcos, M. Garcia, and L. Marroyo, "Dynamic ramp-rate control to smooth short-term power fluctuations in large photovoltaic plants using battery storage systems," in *Proc. 42nd Annu. Conf. IEEE Ind. Electron. Soc.*, 2016, pp. 3052–3057.
- [32] J. Ram, N. Rajasekar, and M. Miyatake, "Design and overview of maximum power point tracking techniques in wind and solar photovoltaic systems: A review," *Renewable Sustain. Energy Rev.*, vol. 73, pp. 1138–1159, Jun. 2017.
- [33] H. D. Tafti, A. Sangwongwanich, Y. Yang, J. Pou, G. Konstantinou, and F. Blaabjerg, "An adaptive control scheme for flexible power point tracking in photovoltaic systems," *IEEE Trans. Power Electron.*, vol. 34, no. 6, pp. 5451–5463, Jun. 2019.
- [34] H. W. Yan, A. Narang, H. D. Tafti, G. G. Farivar, S. Ceballos, and J. Pou, "Minimizing energy storage utilization in a stand-alone dc microgrid using photovoltaic flexible power control," *IEEE Trans. Smart Grid*, vol. 12, no. 5, pp. 3755–3764, Sep. 2021.
- [35] B. Wang, C. Wang, Z. Wang, H. Xue, and S. Ni, "Adaptive energy estimation for supercapacitor based on a real-time voltage state observer in electric vehicle applications," *IEEE Trans. Power Electron.*, vol. 36, no. 7, pp. 7337–7341, Jul. 2021.
- [36] K. S. Ng, C. S. Moo, Y. P. Chen, and Y. C. Hsieh, "Enhanced coulomb counting method for estimating state-of-charge and state-of-health of lithium-ion batteries," *Appl. Energy*, vol. 86, pp. 1506–1511, Sep. 2009.
- [37] Natural Resour. Canada, "High-resolution solar radiation datasets," 2023. [Online]. Available: <https://www.nrcan.gc.ca/energy/renewable-electricity/solar-photovoltaic/18409>



Hein Wai Yan (Graduate Student Member, IEEE) received the B.Eng. degree in electrical and electronic engineering from Nanyang Technological University, Singapore, in 2020, where he is currently working toward the Ph.D. degree in electrical engineering.

His research interests include modulation and control of power converters, energy storage, dc microgrids, and renewable energy systems.



Gaowen Liang (Graduate Student Member, IEEE) received the B.Sc. degree in electrical engineering and automation from the South China University of Technology, Guangzhou, China, in 2018, and the Ph.D. degree in electrical engineering from Nanyang Technological University (NTU), Singapore, in 2022.

He is currently a Research Fellow with Energy Research Institute, NTU (ERI@N). His research interests include multilevel converters, energy storage systems, renewable energy systems, and smart grid.

Dr. Liang was a recipient of the the Second Prize Paper Award at IEEE ECCE in 2022.



Neha Beniwal (Member, IEEE) received the B.Tech. degree in electrical engineering from the National Institute of Technology, Kurukshetra, India, in 2014, the M.Tech. degree in power electronics, electrical machines and drives from the Indian Institute of Technology, Delhi, India, in 2017, and the Ph.D. degree in power electronics from the Interdisciplinary Graduate School, Nanyang Technological University (NTU), Singapore, in 2021.

She is currently a Research Engineer with GE Global Research, Niskayuna, NY, USA. She was a Research Fellow with the Energy Research Institute, NTU (ERI@N). Her research interests include modulation and control of power converters for renewable energy integration, aerospace, and energy storage systems.

Dr. Beniwal was the recipient of the Commendation for Doctorate Research Excellence Award for her outstanding Ph.D. research work by the School of Electrical and Electronic Engineering, NTU, Singapore, the Power System Operation Corporation Ltd. (POSOCO) Power System Award, awarded by POSOCO in association with Foundation for Innovation and Technology Transfer in 2018 for her master's research work, and the Prof. A.K. Sinha Cash Prize and IEEE-PEDES'96 Award at the Annual Convocation of the Indian Institute of Technology Delhi, New Delhi, India, in 2017.



Ezequiel Rodriguez (Member, IEEE) was born in Tarragona, Spain, in 1994. He received the bachelor's degree in electrical engineering and the master's degree in engineering and technology of electronic systems (topping the 2012 and 2016 graduating cohorts as valedictorian) from the Universitat Rovira i Virgili, Tarragona, Spain, in 2012 and 2016, respectively, and the Ph.D. degree in electrical engineering from Nanyang Technological University (NTU), Singapore, in 2022.

He is currently a Research Fellow with Energy Research Institute, NTU(ERI@N), and the Co-Director of the Power Electronics and Applications Research Lab, NTU (PEARL@NTU). His research focuses on the control of power electronic converters, with an emphasis on modular multilevel converters for energy storage and StatCom applications.

Dr. Rodriguez was honored with the 2022 Best Thesis Award by the School of Electrical and Electronic Engineering, NTU, Singapore.



Glen G. Farivar (Senior Member, IEEE) received the B.Sc. degree in electrical engineering from the Nooshirvani Institute of Technology, Babol, Iran, in 2008, the M.Sc. degree in power electronics from the University of Tehran, Tehran, Iran, in 2011, and the Ph.D. degree in electrical engineering from the University of New South Wales, Sydney, NSW, Australia, in 2016.

He is currently a Lecturer with the University of Melbourne, Parkville VIC, Australia. He is also a Co-Founder of SciLeap, a platform dedicated to promoting research integrity, accessibility, and openness. His research interests include renewable energy systems, high power converters, energy storage, flexible ac transmission system, and water electrolysis.



Josep Pou (Fellow, IEEE) received the B.S., M.S., and Ph.D. degrees in electrical engineering from the Technical University of Catalonia (UPC)-Barcelona Tech, Barcelona, Spain, in 1989, 1996, and 2002, respectively.

He is currently a Professor with Nanyang Technological University (NTU), Singapore, where he is Cluster Director of power electronics with the Energy Research Institute, NTU (ERI@N), and Co-Director of the Rolls-Royce at NTU Corporate Lab. In 1990, he joined the faculty of UPC as an Assistant Professor,

where he became an Associate Professor in 1993. From 2013 to 2016, he was a Professor with the University of New South Wales (UNSW), Sydney, NSW, Australia. From 2001 to 2002, and 2005 to 2006, he was a Researcher with the Center for Power Electronics Systems, Virginia Tech, Blacksburg, VA, USA. From 2012 to 2013, he was a Visiting Professor with Australian Energy Research Institute, UNSW. He has authored or coauthored more than 460 published technical papers and has been involved in several industrial projects and educational programs in the fields of power electronics and systems. His research interests include modulation and control of power converters, multilevel converters, renewable energy, energy storage, power quality, HVdc transmission systems, and more-electrical aircraft and vessels.

Dr. Pou is an Associate Editor for IEEE JOURNAL OF EMERGING AND SELECTED TOPICS IN POWER ELECTRONICS. He was the Co-Editor-in-Chief and Associate Editor for IEEE TRANSACTIONS ON INDUSTRIAL ELECTRONICS. He was a recipient of the 2018 IEEE Bimal Bose Award for Industrial Electronics Applications in Energy Systems.